Geometries of the Halocarbene anions HCF− and CF 2−: Ab initio calculation and Franck–Condon analysis

ARTICLE *in* JOURNAL OF MOLECULAR STRUCTURE THEOCHEM · MARCH 2004

Impact Factor: 1.37 · DOI: 10.1016/j.theochem.2003.11.013

ELSEVIER

Journal of Molecular Structure (Theochem) 672 (2004) 133–139

THEO CHEM

www.elsevier.com/locate/theochem

Geometries of the Halocarbene anions HCF^- and CF_2^-: ab initio calculation and Franck–Condon analysis

Jun Liang[a], Xianglei Kong[a], Xianyi Zhang[a], Haiyang Li[a,b,*]

[a]*Laboratory of Environment Spectroscopy, Anhui Institute of Optics and Fine Mechanics, Chinese Academy of Sciences, Hefei 230031, People's Republic of China*

[b]*Dalian Institute of Chemical Physics, Chinese Academy of Science, Dalian 116023, People's Republic of China*

Received 21 September 2003; revised 11 November 2003; accepted 12 November 2003

Abstract

A theoretical method to calculate multidimensional Franck–Condon factors including Duschinsky effects is described and used to simulate the photoelectron spectra of HCF^- and CF_2^- radicals. Geometry optimization and harmonic vibrational frequency calculations have been performed on the $\tilde{X}^1A'$ state of HCF and $\tilde{X}^2A''$ state of HCF^-, and $\tilde{X}^1A_1$ state of CF_2 and $\tilde{X}^2B_1$ state of CF_2^-. Franck–Condon analyses and spectral simulation were carried out on the first photoelectron band of HCF^- and CF_2^-, respectively. The theoretical spectra obtained by employing B3LYP/6-311 + G(2d,p) values are in excellent agreement with the observed ones. In addition, the equilibrium geometry parameters, R(CF) = 0.1475 ± 0.0005 nm, of the $\tilde{X}^2A''$ state of HCF^-, and r(FC) = 0.1425 ± 0.0005 nm and ∠(FCF) = 100.5 ± 0.5°, of the $\tilde{X}^2B_i$ state of CF_2^-, are derived by employing an iterative Franck–Condon analysis procedure in the spectral simulation.

Keywords: Ab initio calculations; Franck–Condon analysis; Spectral simulation; Anions

1. Introduction

Recently, we have determined the geometries of the anions HNO^- and DNO^- by applying Franck–Condon (FC) analyses to their photoelectron spectra [1]. In the study, the ab initio force constants were used in FC analysis via the reduced-mass-weighted atom displacement matrix as obtained from an ab initio frequency calculation. With quantum chemical computing programs being readily available, geometries and normal modes of small to medium size molecules in different electronic states can now be calculated routinely. Based on these methods, numerous applications of FC calculations have been presented in the literature [1–13], and most of these studies just focus on the interpretation of experimentally known spectra. Because the geometry difference between two electronic states is a major factor that influences FC intensities, the simulation of vibronic spectra of ployatomic molecules can be regarded as a valuable test with respect to the quality of calculated geometries and as a starting point to obtain improved structures. In addition, spectral simulations of vibrational structure based on computed Franck–Condon factors (FCF) could provide fingerprint type identification of an observed spectrum, in terms of both the carrier and the electronic states in the transition (see, for examples, Refs. [8,9], and references therein). Also, it has been demonstrated that spectral simulations can be very useful in establishing vibrational assignments in an electronic spectrum observed with complex vibrational structure [1–4,6,9,10]. Moreover, even if the electronic spectrum is not rotationally resolved, if the geometrical parameters of one of the electronic states is well established by, for example, microwave spectroscopic measurements, the geometrical parameters of the other state can be determined by estimating the geometry change between the states by the iterative Franck–Condon analysis (IFCA) method [1–4,6–13].

For many years, simple substituted halocarbenes are of considerable current interest from both theoretical and experimental points of view because of their important role in many organic and organometallic reactions [14,15]. There have been many theoretical and experimental studies on HCF and CF_2 [16–26]. In contrast, their anions HCF^- and CF_2^- are not so well characterized. In this paper,

* Corresponding author. Tel./fax: +86-551-559-1550.
E-mail address: hli@aiofm.ac.cn (H. Li).

0166-1280/$ - see front matter © 2003 Elsevier B.V. All rights reserved.
doi:10.1016/j.theochem.2003.11.013

geometry optimization and harmonic vibrational frequency calculations were performed on the $\tilde{X}^1A'$ state of HCF and $\tilde{X}^2A''$ state of HCF^-, and $\tilde{X}^1A_1$ state of CF_2 and $\tilde{X}^2B_1$ state of CF_2^-. FC analyses and spectral simulation were carried out on the first photoelectron band of HCF^- and CF_2^- (i.e. $\tilde{X}^1A' - \tilde{X}^2A''$ and $\tilde{X}^1A_1 - \tilde{X}^2B_1$ transitions) [16], respectively. In addition, employing the IFCA procedure in the spectral simulation, the equilibrium geometries of the $\tilde{X}^2A''$ state of HCF^- and $\tilde{X}^2B_1$ state of CF_2^- are derived, respectively.

2. Theoretical method

Different methods [27–33] have been proposed to calculate multidimensional FC integrals. We chose the multidimensional generating function method described by Sharp and Rosenstock [28] for the integrals. First, the Duschinsky effect, or mode mixing of the initial and final electronic states, is expressed as:

$$\mathbf{Q}' = \mathbf{JQ} + \mathbf{K} \tag{1}$$

where the $\mathbf{Q}$ and $\mathbf{Q}'$ are the normal coordinates of the two electronic states, respectively, and the matrix $\mathbf{J}$ and column vector $\mathbf{K}$ define the linear transformation. To obtain the matrix $\mathbf{J}$ and vector $\mathbf{K}$ in Eq. (1), in terms of Cartesian coordinates displacements [34–36], the general linear transformation of an arbitrary distortion $\mathbf{X}$ can be written:

$$\mathbf{X}' = \mathbf{ZX} + \mathbf{R} \tag{2}$$

where $\mathbf{X}$ and $\mathbf{X}'$ are distortions expressed as Cartesian displacements from the equilibrium geometries of the anion and neutral, respectively. $\mathbf{R} = \mathbf{ZR}_{eq} - \mathbf{R}'_{eq}$ is the change in equilibrium geometry between the anion and the neutral in Cartesian coordinates centered on the molecular center of mass, and $\mathbf{Z}$ is a rotation matrix, which is a unit matrix for most molecules of C_{2V} or higher symmetry ($\mathbf{Z} = 1$). In a conventional normal-mode analysis, the Cartesian displacements, $\mathbf{X}$, are transformed to internal coordinates, $\mathbf{S}$, and then to normal coordinates, $\mathbf{Q}$, and visa versa, by the $\mathbf{B}$ and $\mathbf{L}$ matrices. That is $\mathbf{S} = \mathbf{BX}$ and $\mathbf{S} = \mathbf{LQ}$. The definitions of $\mathbf{B}$ and $\mathbf{L}$ are consistent with Ref. [28]. After several substitutions, the relation to relate $\mathbf{Q}$ to $\mathbf{Q}'$ is obtained as:

$$\mathbf{Q}' = (\mathbf{L}'^{-1}\mathbf{B}')[\mathbf{ZM}^{-1}(\mathbf{L}^{-1}\mathbf{B})^{\dagger}\mathbf{Q} + \mathbf{R}] \tag{3}$$

where the superscript '†' indicates the transpose of the matrix. Eq. (3), substituted back into Eq. (1) gives expressions for $\mathbf{J}$ and $\mathbf{K}$:

$$\mathbf{J} = (\mathbf{L}'^{-1}\mathbf{B}')\mathbf{ZM}^{-1}(\mathbf{L}^{-1}\mathbf{B})^{\dagger} \text{ and } \mathbf{K} = (\mathbf{L}'^{-1}\mathbf{B}')\mathbf{R} \tag{4}$$

Having carried out the vibrational analyses for both the initial and final electronic states to obtain $\mathbf{B}$, $\mathbf{L}$, $\mathbf{B}'$ and $\mathbf{L}'$, one can use Eq. (4) for a description of the Duschinsky effect that is valid even for large changes in geometry or force constants.

The Cartesian atom displacement matrix (ADM) is defined as [37]

$$\text{ADM} = \mathbf{M}^{-1}(\mathbf{L}^{-1}\mathbf{B})^{\dagger} \tag{5}$$

which relates $\mathbf{Q}$ to $\mathbf{X}$. $\mathbf{M}$ is a diagonal matrix with the atomic masses on the diagonal.

For a molecule of N atoms, if we define a $3N \times 3N - 6$ matrix, **g03**, containing the normal mode output from GAUSSIAN**03** [38], and a $3N - 6 \times 3N - 6$ diagonal matrix, $\mathbf{V}$, containing the reduced masses for each mode on the diagonal, then

$$\text{ADM} = (\mathbf{g03})\mathbf{V}^{-1/2} \tag{6}$$

which removes the reduced-mass weighting. Finally, Using Eqs. (4)–(6), $\mathbf{J}$ and $\mathbf{K}$ in terms of the GAUSSIAN**03** output for the two electronic states are given by:

$$\mathbf{J} = [\mathbf{M}(\mathbf{g03}')\mathbf{V}'^{-1/2}]^{\dagger}\mathbf{Z}(\mathbf{g03})\mathbf{V}^{-1/2} \text{ and } \mathbf{K} = [\mathbf{M}(\mathbf{g03}')\mathbf{V}'^{-1/2}]^{\dagger}\mathbf{R} \tag{7}$$

where, as usual, unprimed and primed quantities refer to the initial state and the final state in the transition, respectively. Having then computed $\mathbf{J}$ and $\mathbf{K}$, the FCFs are easily produced using the algebraic expressions below. Following Sharp et al. [28], the arrays $\mathbf{A}$ through $\mathbf{E}$ are defined in terms of the Duschinsky rotations arrays, $\mathbf{J}$ and $\mathbf{K}$, and the harmonic frequencies. A diagonal matrix $\mathbf{\Gamma}$ has the harmonic frequencies as diagonal elements. If FCFs are computed for a vibrationally cold molecule, i.e. no hot bands, then only $\mathbf{C}$ and $\mathbf{D}$ are necessary:

$$\mathbf{A} = 2\mathbf{\Gamma}'^{1/2}\mathbf{J}[\mathbf{J}^{\dagger}\mathbf{\Gamma}'\mathbf{J} + \mathbf{\Gamma}]^{-1}\mathbf{J}^{\dagger}\mathbf{\Gamma}'^{1/2} - \mathbf{1} \tag{8a}$$

$$\mathbf{B} = -2\mathbf{\Gamma}'^{1/2}[\mathbf{J}(\mathbf{J}^{\dagger}\mathbf{\Gamma}'\mathbf{J} + \mathbf{\Gamma})^{-1}\mathbf{J}^{\dagger}\mathbf{\Gamma}' - \mathbf{1}]\mathbf{K} \tag{8b}$$

$$\mathbf{C} = 2\mathbf{\Gamma}^{1/2}[\mathbf{J}^{\dagger}\mathbf{\Gamma}'\mathbf{J} + \mathbf{\Gamma}]^{-1}\mathbf{\Gamma}^{1/2} - \mathbf{1} \tag{8c}$$

$$\mathbf{D} = -2\mathbf{\Gamma}^{1/2}[\mathbf{J}^{\dagger}\mathbf{\Gamma}'\mathbf{J}^{-1} + \mathbf{\Gamma}]^{-1}\mathbf{J}^{\dagger}\mathbf{\Gamma}'\mathbf{K} \tag{8d}$$

$$\mathbf{E} = 4\mathbf{\Gamma}^{1/2}[\mathbf{J}^{\dagger}\mathbf{\Gamma}'\mathbf{J} + \mathbf{\Gamma}]^{-1}\mathbf{J}^{\dagger}\mathbf{\Gamma}'^{1/2} \tag{8e}$$

The more general algebraic expressions were given by Chen [37], with m quanta in mode i and n quanta in mode j. The FCFs are:

$$\text{FCF}(m,n) = \frac{m!n!}{2^{m+n}}\left[\sum_{p=0}^{\binom{m}{n}}\sum_{q=0}^{\left\{\frac{m-p}{2}\right\}}\sum_{r=0}^{\left\{\frac{n-p}{2}\right\}}\frac{2^p D_i^{m-2q-p} D_j^{n-2r-p} C_{ii}^q C_{jj}^r C_{ij}^p}{p!q!r!(m-2q-p)!(n-2r-p)!}\right]^2 \tag{9}$$

The limit for the outermost summation is the lesser of the two numbers, m and n. The bracketed expressions for the limits of the remaining two summations are taken to mean the greatest integer less than or equal to $(m-p)/2$ or $(n-p)/2$.

3. Computational details

Geometry optimization and harmonic vibrational frequency calculations were carried out on the $\tilde{X}^1A'$ and $\tilde{X}^1A_1$ states of the neutral molecule HCF and CF_2, and$\tilde{X}^2A''$ and $\tilde{X}^2B_1$ state of the negative ion HCF^- and CF_2^- at the B3LYP, QCISD, QCISD(T), CCSD and CCSD(T) levels with the 6-311 + G(2d,p) basis sets. The B3LYP, QCISD, QCISD(T), CCSD and CCSD(T) calculations were performed employing the GAUSSIAN**03** suite of programs [38].

FCF calculations on the $\tilde{X}^1A' - \tilde{X}^2A''$ and $\tilde{X}^1A_1 - \tilde{X}^2B_1$ photodetachment were carried out, employing B3LYP/6-311 + G(2d,p) force constants, initially (see later text), B3LYP/6-311 + G(2d,p) geometry for the electronic ground state $\tilde{X}^2A''$ of the HCF^- and $\tilde{X}^2B_1$ of the CF_2^-, and experimental geometries of the neutral HCF and CF_2 for the electronic state $\tilde{X}^1A'$ and $\tilde{X}^1A_1$, respectively. The theoretical method used in the FCF calculations has been described in the Section 2. Briefly, the harmonic oscillator model was employed and Duschinsky rotation was included in the FCF calculations. The computed FCFs were then used to simulate the vibrational structure of the $\tilde{X}^1A' - \tilde{X}^2A''$ and $\tilde{X}^1A_1 - \tilde{X}^2B_1$ photodetachment spectra of HCF^- and CF_2^-, respectively, employing a Gaussian line-shape and a full-width-at-half-maximum (FWHM) of 300 cm^{-1} for the $\tilde{X}^1A' - \tilde{X}^2A''$ detachment and a FWHM of 270 cm^{-1} for the $\tilde{X}^1A_1 - \tilde{X}^2B_1$ detachment, respectively.

In order to obtain a reasonable match between the simulated and observed spectra, the IFCA procedure [37] was also carried out, where the ground state geometrical parameters of the HCF and CF_2 molecules were fixed to the experimental values for the $\tilde{X}^1A' - \tilde{X}^2A''$ and $\tilde{X}^1A_1 - \tilde{X}^2B_1$ photo-detachment processes, respectively, while the ground state geometrical parameters of the HCF^- and CF_2^- were varied systematically. Thus, the ground state geometrical parameters of the HCF^- and CF_2^- were varied until a best match between the simulated and observed spectra was obtained.

4. Results and discussions

4.1. Geometry optimization and frequency calculations

The optimized geometric parameters and computed vibrational frequencies for the $\tilde{X}^1A'$ states of HCF and $\tilde{X}^2A''$ state of HCF^- and $\tilde{X}^1A_1$ states of CF_2 and $\tilde{X}^2B_1$ states of CF_2^- as obtained in this work are listed in Tables 1–4. The theoretical and/or experimental values available in the literatures are also included for comparison. The bending vibration is denoted ω_2, according to the convention for triatomic molecules.

From Table 1, for the $\tilde{X}^1A'$ state of HCF, the computed bond lengths and angles obtained at different levels of calculation seems to be highly consistent. For R(HC), R(CF) and ∠(HCF), the largest deviations between calculated and experimental bond lengths and angles are less than 0.0008, 0.002 nm and 1.0°, respectively, (see Table 1). The estimated values based on density functional theory at the B3LYP/6-311 + G(2d,p) level, are 0.11225, 0.13125 nm and 102.071°. The differences between the calculated and experimental values are only 0.00075, 0.00075 nm and 0.918° for R(HC), R(CF) and ∠(HCF), respectively. Both the optimized geometric parameters and the vibrational frequencies calculated at B3LYP/6-311 + G(2d,p) level gave the best agreement with the corresponding available experimental values, and were therefore utilized in subsequent FC analyses and spectral simulation.

From Table 2, for the state $\tilde{X}^2A''$ of HCF^-, the computed bond lengths and angles obtained at different levels of

Table 1
Summary of some computed and experimental geometrical parameters and vibrational frequencies (cm^{-1}) of the $\tilde{X}^1A'$ state of HCF obtained at different levels of calculation

Method	R(HC) (nm)	R(CF) (nm)	∠(HCF) (°)	ω_1 (H–C)	ω_2 (bend)	ω_3 (C–F)
B3LYP/6-311 + G(2d,p)	0.11225	0.13125	102.071	2778.7	1441.0	1181.1
QCISD/6-311 + G(2d,p)	0.11225	0.13150	102.166	2809.6	1448.5	1187.5
QCISD(T)/6-311 + G(2d,p)	0.11248	0.13191	102.104	2783.0	1433.9	1170.8
CCSD/6-311 + G(2d,p)	0.11222	0.13118	102.233	2815.0	1452.5	1206.1
CCSD(T)/6-311 + G(2d,p)	0.11246	0.13174	102.143	2786.1	1436.4	1180.6
CEPA[a]	0.1120	0.1309	102.3	2799	1441	1215
MRCI + Dav/aug-cc-pVTZ[b]	0.1122	0.1324	101.9	2803	1431	1190
MRCI + Dav/cc-pVQZ[b]	0.1121	0.1309	102.3	2799	1433	1179
CCSD(T)/cc-pVQZ[b]	0.1121	0.1309	102.3	2804	1430	1175
Expt.	0.1130(3)[c]	0.1305(3)[c]	103.0(5)[c]	2643.04[c]	1403.20[c]	1189(25)[d]

[a] From Ref. [17].
[b] From Ref. [18].
[c] From Ref. [19].
[d] From Ref. [20].

Table 2
Summary of some computed and experimental geometrical parameters and vibrational frequencies (cm^{-1}) of the $\tilde{X}^2A''$ state of HCF^- obtained at different levels of calculation

Method	R(HC) (nm)	R(CF) (nm)	∠(HCF) (°)	ω_1 (H–C)	ω_2 (bend)	ω_3 (C–F)
B3LYP/6-311 + G(2d,p)	0.11287	0.14863	98.834	2634.0	1265.8	710.2
QCISD/6-311 + G(2d,p)	0.11294	0.14860	98.944	2673.1	1278.5	727.2
QCISD(T)/6-311 + G(2d,p)	0.11322	0.14914	98.815	2643.9	1263.7	715.1
CCSD/6-311 + G(2d,p)	0.11294	0.14806	99.078	2673.9	1285.0	745.1
CCSD(T)/6-311 + G(2d,p)	0.11320	0.14896	98.955	2645.9	1265.3	720.7
Expt.						720(25)[a]

[a] From Ref. [16].

calculation seem to be highly consistent. Because no experimental geometric values are available for comparison, it is expected that the geometrical parameters obtained at the higher levels of calculation should be the more reliable. Regarding the computed vibrational frequencies, for the state $\tilde{X}^2A''$ of HCF^-, the values obtained at the various levels are reasonably consistent, especially with respect to the stretching F–C mode ω_3 (see Table 2). The frequency difference between the B3LYP and experimental value is 5.6 cm^{-1}. The B3LYP/6-311 + G(2d,p) results are the best overall agreement to the corresponding available experimental and other theoretical values, and were therefore utilized in subsequent FC analyses and spectral simulations.

From Table 3, for the state $\tilde{X}^1A_1$ of CF_2, the computed bond lengths and angles obtained at different levels of calculation seem to be highly consistent. For r(FC) and ∠(FCF), the largest deviations between calculated and experimental bond lengths and angles are less than 0.0009 nm and 0.3°, respectively, (see Table 3). The estimated values based on density functional theory at the B3LYP/6-311 + G(2d,p) level, are 0.13073 nm and 104.476°. The differences between calculated and experimental values are only 0.00073 nm and 0.46° for r(FC) and ∠(FCF), respectively. Both the optimized geometric parameters and the vibrational frequencies calculated at B3LYP/6-311 + G(2d,p) level gave the better agreement with the corresponding available experimental values, and were therefore utilized in subsequent FC analyses and spectral simulation.

From Table 4, for the state $\tilde{X}^2B_1$ of CF_2^-, the computed bond lengths and angles obtained at different levels of calculation seem to be highly consistent. Because no experimental geometric values are available for comparison, it is expected that the geometrical parameters obtained at the higher levels of calculation should be the more reliable. Regarding the computed vibrational frequencies, for the state $\tilde{X}^2B_1$ of CF_2^-, the values obtained at the various levels are reasonably consistent, especially with respect to the symmetrical stretching mode ω_1 (see Table 4). The frequency difference between the B3LYP and experimental value is 9.4 cm^{-1}. The B3LYP/6-311 + G(2d,p) results are the best overall agreement to the corresponding available experimental and theoretical values, and were therefore utilized in subsequent FC analyses and spectral simulations.

4.2. Franck–Condon simulations

4.2.1. HCF ($\tilde{X}^1A'$)—HCF^-($\tilde{X}^2A''$) detachment

For the $\tilde{X}^1A' - \tilde{X}^2A''$ detachment, the simulated photoelectron spectrum of HCF^- is shown in Fig. 1(b) with

Table 3
Summary of some computed and experimental geometrical parameters and vibrational frequencies (cm^{-1}) of the $\tilde{X}^1A_1$ state of CF_2 obtained at different levels of calculation

Method	r(FC) nm	∠(FCF) (°)	ω_1 (a_1)	ω_2 (a_1)	ω_3 (b_2)
B3LYP/6-311 + G(2d,p)	0.13051	104.692	1210.1	666.9	1083.4
QCISD/6-311 + G(2d,p)	0.13033	104.776	1233.1	671.2	1123.9
QCISD(T)/6-311 + G(2d,p)	0.13087	104.760	1209.9	658.8	1096.8
CCSD/6-311 + G(2d,p)	0.13004	104.828	1250.3	677.3	1138.7
CCSD(T)/6-311 + G(2d,p)	0.13072	104.790	1219.0	661.9	1104.9
MP2/6-311 + G(2df)[a]	0.1298	105.0	1261	679	1151
CASPT/cc-pVTZ[b]	0.1300	105.2	1245.4	671.0	1163.0
CCSD(T)/cc-pVTZ[b]	0.1303	104.9	1255.2	672.9	1162.5
CCSD(T)/aug-cc-pVQZ[c]	0.12981	104.85			
Expt.	0.1300[d]	104.94[d]	1225.0793[e]	666.24922[e]	1114.4435[e]

[a] From Ref. [11].
[b] From Ref. [21].
[c] From Ref. [22].
[d] From Ref. [23].
[e] From Ref. [24].

Table 4
Summary of some computed and experimental geometrical parameters and vibrational frequencies (cm^{-1}) of the $\tilde{X}^2B_1$ state of CF_2^- obtained at different levels of calculation

Method	r(FC) (nm)	∠(FCF) (°)	ω_1 (a_1)	ω_2 (a_1)	ω_3 (b_2)
B3LYP/6-311 + G(2d,p)	0.14495	100.280	850.6	470.9	665.6
QCISD/6-311 + G(2d,p)	0.14454	99.981	874.8	484.2	709.2
QCISD(T)/6-311 + G(2d,p)	0.14527	100.063	854.9	470.9	686.0
CCSD/6-311 + G(2d,p)	0.14417	100.024	889.0	490.5	724.1
CCSD(T)/6-311 + G(2d,p)	0.14509	100.079	861.5	474.0	692.5
MP2(Full)/6-311 + G*[a]	0.144	100.30			
LDA[b]	0.1445	99.6			
Expt.			860(30)[c]		

[a] From Ref. [25].
[b] From Ref. [26].
[c] From Ref. [16].

the experimental observed photoelectron spectrum shown in Fig. 1(a). Vibrational assignments for the stretching mode ω_3 of the neutral molecule HCF are also provided, with the label $(0,0,n-0,0,0)$ corresponding to $(0,0,\omega_3-0,0,0)$ transition (see Fig. 1(b)). The computed FCFs for the H–C stretching ω_1 and the H–C–F bending ω_2 modes were found to be negligibly small, therefore the ω_1 and ω_2 mode are not included in the assignment. In spectral simulation, a FWHM

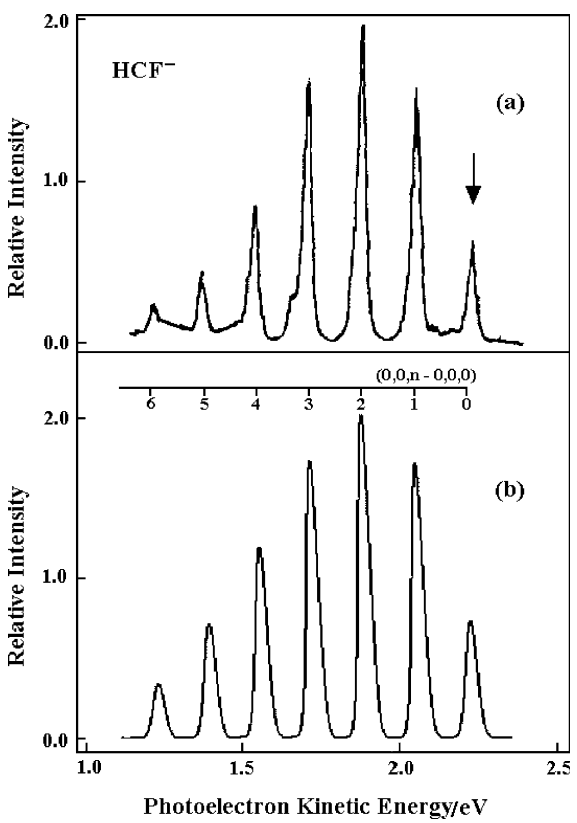

Fig. 1. (a) The experimental photoelectron spectrum of HCF^- (from Ref. [16]) and (b) the simulated spectrum with vibrational assignments provided for the $\tilde{X}^1A' - \tilde{X}^2A''$ detachment process. The FWHM used for the components of the simulated spectra is 300 cm^{-1}.

of 300 cm^{-1} was utilized with Gaussian band envelopes for HCF. This quantity is almost equal to that of the corresponding experimental spectrum. The relative intensities were chosen to match the first vibronic profile between 1.0 and 2.5 eV in the experimental spectra (Ref. [16]).

It was also found that the computed photoelectron spectrum of HCF^- for the $\tilde{X}^1A' - \tilde{X}^2A''$ detachment is almost identical to the experimental spectra. This suggests that for the ground electronic state of HCF, the computed geometry changes upon detachment at the B3LYP/6-311 + G(2d,p) level are highly accurate, and the harmonic model seems to be reasonably adequate in this case. However, it can be seen from Fig. 1(a) and (b) that the match is far from perfect. Comparing the simulated spectrum in Fig. 1(b) and the experimental one in Fig. 1(a), it can be seen that reasonably good agreements are obtained mainly for the vibrational peaks with low quantum numbers. Discrepancies between simulation and observation become larger for peaks with higher quantum numbers. This is mainly due to anharmonicity effects not included in the FCF calculation. With vibrational quantum numbers increasing, the stronger the anharmonicity effect is and the greater the influence on the simulated spectra. This is also true for other molecules, especially those containing a hydrogen atom [1,7,11].

The variations of geometries of the molecule between the electronic states using the IFCA method [1–4,6–13] would yield better matches between the simulated and observed spectra than that obtained with the B3LYP/6-311 + G(2d,p) geometries. A reasonably reliable bond length of R(CF) for the ground state $\tilde{X}^2A''$ of HCF^- can be deduced based on the experimental structural parameters of HCF in the $\tilde{X}^1A'$ state and the computed geometry changes upon photodetachment at the B3LYP/6-311 + G(2d,p) level. For $\tilde{X}^2A'' - \tilde{X}^1A'$ photodetachment spectrum, the latter values were shown to be reliable from the excellent agreement between the simulated and observed spectra as mentioned above. Hence, by using the IFCA method, the best IFCA bond length R(CF) obtained for the $\tilde{X}^2A''$ state of HCF^-, employing the B3LYP/6-311 + G(2d,p) force constants, is 0.1475 ± 0.0005 nm.

It should be noted that since no H–C stretching and H–C–F bending structures (i.e. structure in ω_1 and ω_2), are observed in the first profiles (in the experimental spectra of Ref. [14]) for both states of interest, the computed R(HC) bond length and ∠(HCF) bond angle changes from the B3LYP calculations was assumed in the IFCA procedure. In view of the near-perfect match between the best-simulated spectrum and the observed spectrum, we anticipate the B3LYP R(HC) and ∠(HCF) changes to be close to the real one.

4.2.2. CF_2 ($\tilde{X}^1A_1$)—CF_2^- ($\tilde{X}^2B_1$) detachment

For the $\tilde{X}^1A_1 - \tilde{X}^2B_1$ photodetachment, the simulated photoelectron spectrum of CF_2^- are shown in Fig. 2(b), with the experimental observed photoelectron spectrum shown in Fig. 2(a). Vibrational assignments for the symmetric

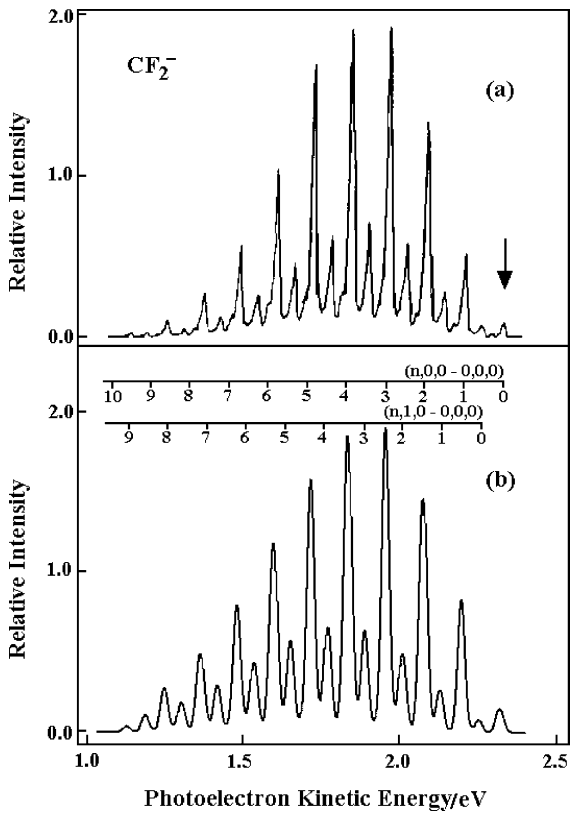

Fig. 2. (a) The experimental photoelectron spectrum of CF_2^- (from Ref. [16]) and (b) the simulated spectrum with vibrational assignments provided for the $\tilde{X}^1A_1 - \tilde{X}^2B_1$ detachment process. The FWHM used for the components of the simulated spectra is 270 cm^{-1}.

stretching ω_1 and bending ω_2 modes of the neutral molecule CF_2 are also provided, respectively, with the label $(n,0,0-0,0,0)$ and $(n,1,0-0,0,0)$ corresponding to the $(\omega_1, \omega_2,0,-0,0,0)$ transition. From the harmonic calculation, it was found that the FCFs for transitions involving the asymmetric stretching mode ω_3 are negligibly small and therefore the ω_3 mode is not included in the assignments. In the spectral simulation, a FWHM of 270 cm^{-1} was utilized with Gaussian band envelopes for CF_2. The relative intensities were chosen to match the vibronic profile between 1.0 and 2.5 eV in the experimental spectra (Ref. [16]).

It was found that the computed photoelectron spectrum of CF_2^- for the $\tilde{X}^1A_1 - \tilde{X}^2B_1$ detachment is almost identical to the experimental spectra. This suggests that the computed geometry changes upon detachment at the B3LYP/6-311 + G(2d,p) level are highly accurate, and the harmonic model seems to be reasonably adequate. However, discrepancies between simulation and observation become larger for peaks with higher quantum numbers. This is mainly due to anharmonicity effects not included in the FCF calculation. With vibrational quantum numbers increasing, the stronger the anharmonicity effect is and the greater the influence on the simulated spectra.

By using the same IFCA method above, reasonably reliable bond length r(FC) and bond angle ∠(FCF) for the ground state $\tilde{X}^2B_1$ state of CF_2^- can be deduced based on the experimental structural parameters of CF_2 in the $\tilde{X}^1A_1$ state and the computed geometry changes upon photodetachment at the B3LYP/6-311 + G(2d,p) level. For the $\tilde{X}^1A_1 - \tilde{X}^2B_1$ photodetachment spectrum, the latter values were shown to be reliable from the excellent agreement between the simulated and observed spectra (see Fig. 2). Hence, by using the IFCA method, the best IFCA bond length r(FC) and bond angle ∠(FCF) obtained for the ground state $\tilde{X}^2B_1$ state of CF_2^-, employing the B3LYP/6-311 + G(2d,p) force constants, are 0.1425 ± 0.0005 nm and 100.5 ± 0.5°, respectively.

5. Conclusion

In the present study, attempts have been made to simulate the observed HCF $(\tilde{X}^1A')$—$HCF^-(\tilde{X}^2A'')$ and CF_2 $(\tilde{X}^1A_1)$—$CF_2^-(\tilde{X}^2B_1)$ detachment photoelectron spectra, respectively, using a harmonic model and including Duschinsky effects. In the case of the photoelectron spectra of the $\tilde{X}^1A' - \tilde{X}^2A''$ and $\tilde{X}^1A_1 - \tilde{X}^2B_1$ detachments, it seems that the harmonic model is reasonably adequate. The rather reliable bond length R(CF), r(FC) and bond angle ∠(FCF) were obtained for the first time, through the IFCA procedure. Based on the sensitivity of the relative intensities towards the variation of the bond length and bond angle, the uncertainties in the R(CF)/r(FC) and ∠(FCF) are probably around ± 0.0005 nm and ± 0.5°, respectively. Nevertheless, focusing on the relative intensities of the vibrational peaks with higher state quantum numbers, the FC simulated spectra are not reasonably consistent with the experimental spectra. Clearly, anharmonicity should be incorporated into the model for computing FCFs in order to achieve better agreement between simulation and observation. A simple way to include anharmonicity in an FCF calculation is to express the anharmonic vibrations as linear combinations of the products of harmonic oscillator functions. In this way, the anharmonic vibrational FCF can be reduced to a sum of harmonic overlap integrals, which can be evaluated readily with available analytical formulas. Botschwina and coworkers are one of the few research groups performing anharmonic FCF calculations in this way [39]. Recently, details of a few other types of anharmonic FCF methods have been published [3,6,40–42]. FC factor calculations that consider anharmonicity effects will be our future work.

Acknowledgements

This work was supported by the National Natural Science Foundation of China (No. 20073042) and the Natural Science Foundation of Anhui province (No.2001kj263zc), and the Director Research Grants (2003) of Hefei Institute of Physical Science and Anhui Institute of Optics and Fine Mechanics, Chinese Academy of Science.

References

[1] J. Liang, X. Kong, X. Zhang, H. Li, Chem. Phys. 294 (2003) 85.
[2] E.P.F. Lee, D.K.W. Mok, J.M. Dyke, F.T. Chau, J. Phys. Chem. A106 (2002) 10130.
[3] F.T. Chau, J.M. Dyke, E.P.F. Lee, D.K.W. Mok, J. Chem. Phys. 115 (2001) 5816.
[4] D.C. Wang, F.T. Chau, D.K.W. Mok, E.P.F. Lee, L. Beeching, J.S. Ogden, J.M Dyke, J. Chem. Phys. 114 (2001) 10682.
[5] S. Schumm, M. Gerhards, K. Kleinermanns, J. Phys. Chem. A104 (2000) 10648.
[6] D.K.W. Mok, E.P.F. Lee, F.T. Chau, D.C. Wang, J.M. Dyke, J. Chem. Phys. 113 (2000) 5791.
[7] E.P.F. Lee, D.K.W. Mok, J.M. Dyke, F.T. Chau, Chem. Phys. Lett. 340 (2001) 348.
[8] F.T. Chau, E.P.F. Lee, D.K.W. Mok, D.C. Wang, J.M. Dyke, J. Electron, Spectrosc. Relat. Phenom. 108 (2000) 75.
[9] J.M. Dyke, S.D. Gamblin, N. Hooper, E.P.F. Lee, A. Morris, D.K.W. Mok, F.T. Chau, J. Chem. Phys. 112 (2000) 6262.
[10] F.T. Chau, D.C. Wang, E.P.F. Lee, J.M. Dyke, D.K.W. Mok, J. Phys. Chem. A103 (1999) 4925.
[11] F.T. Chau, J.M. Dyke, E.P.F. Lee, D.C. Wang, J. Electron, Spectrosc. Relat. Phenom. 97 (1998) 33.
[12] F.T. Chau, E.P.F. Lee, D.C. Wang, J. Phys. Chem. A101 (1997) 1603.
[13] E.P.F. Lee, J.M. Dyke, D.K.W. Mok, R.P. Claridge, F.T. Chau, J. Phys. Chem. A105 (2001) 9533.
[14] E.R. Davidson, in: W.T. Barden (Ed.), Diradicals, Wiley, New York, 1982.
[15] D.L.S. Brahms, W.P. Dailey, Chem. Rev. 96 (1996) 1585.
[16] K.K. Murray, D.G. Leopold, T.M. Miller, W.C. Lineberger, J. Chem. Phys. 89 (1988) 5442.
[17] B. weis, P. Rosmus, K. Yamashita, K. Morokuma, J. Chem. Phys. 92 (1990) 6635.
[18] T.W. Schmidt, G.B. Bacskay, S.H. Kable, Chem. Phys. Lett. 292 (1998) 80.
[19] T. Suzuki, E. Hirota, J. Chem. Phys. 88 (1988) 6778.
[20] M.K. Gilles, K.M. Ervin, J. Ho, W.C. Lineberger, J. Phys. Chem. 96 (1992) 1130.
[21] K. Sendt, G.B. Bacskay, J. Chem. Phys. 112 (2000) 2227.
[22] J. Breidung, W. Thiel, J. Mol. Spectrosc. 205 (2001) 28.
[23] C.W. Matthews, Can. J. Phys. 45 (1967) 2355.
[24] M.R. Cameron, S.H. Kable, G.B. Bacskay, J. Chem. Phys. 103 (1995) 4476.
[25] R.L. Schwartz, G.E. Davico, T.M. Ramond, W.C. Lineberger, J. Phys. Chem. A103 (1999) 8213.
[26] G.L. Gutsev, T. Ziegler, J. Phys. Chem. 95 (1991) 1220.
[27] J.B. Coon, R.E. Dewames, C.M. Loyd, J. Mol. Spectrosc. 8 (1962) 285.
[28] T.E. Sharp, H.M. Rosenstock, J. Chem. Phys. 41 (1964) 3453.
[29] H. Kupka, P.H. Cribb, J. Chem. Phys. 85 (1986) 1303.
[30] E.V. Doktorov, I.A. Malkin, V.I. Manko, J. Mol. Spectrosc. 56 (1975) 1.
[31] E.V. Doktorov, I.A. Malkin, V.I. Manko, J. Mol. Spectrosc. 64 (1977) 302.
[32] T.R. Faulkner, F.S. Richardson, J. Chem. Phys. 70 (1979) 1201.
[33] K.M. Chen, C.C. Pei, Chem. Phys. Lett. 165 (1990) 532.
[34] A. Warshel, J. Chem. Phys. 62 (1975) 214.
[35] A. Warshel, M. Karplus, Chem. Phys. Lett. 17 (1972) 7.
[36] A. Warshel, M. Karplus, J. Am. Chem. Soc. 96 (1974) 5677.
[37] P. Chen, in: C.Y. Ng, T. Baer, I. Powis (Eds.), Photoelectron spectroscopy of reactive intermediates, Unimolecular and Bimolecular Reaction Dynamics, Wiley, New York, 1994, p. 371.
[38] M.J. Frisch, G.W. Trucks, H.B. Schlegel, G.E. Scuseria, M.A. Robb, J.R. Cheeseman, V.G. Zakrzewski, J.A. Montgomery, R.E. Stratmann, J.C. Burant, S. Dapprich, J.M. Millam, A.D. Daniels, K.N. Kudin, M.C. Strain, O. Farks, J. Tomasi, V. Barone, M. Cossi, R. Cammi, B. Mennucci, C. Pomelli, C. Adamo, S. Cliffoird, J. Ochterski, G.A. Petersson, P.Y. Ayala, Q. Cui, K. Morokuma, D.K. Malick, A.D. Rabuck, K. Raghavachari, J.B. Foresman, J. Cioslowski, J.V. Ortiz, B.B. Stefanov, G. Liu, A. Liashenko, P. Piskorz, I. Komaromi, R. Gomperts, R.L. Martin, D.J. Fox, T. Keith, M.A. Al-Laham, C.Y. Peng, A. Nanayakkara, C. Gonzalez, M. Challacombem, P.M.W. Gill, B.G. Johnson, W. Chen, M.W. Wong, J.L. Andres, M. Head-Gordon, E.S. Replogle and J.A. Pople, GAUSSIAN03, Gaussian, Inc., Pittsburgh, PA, 2003.
[39] P. Botschwina, B. Schulz, M. Horn, M. Matuschewski, Chem. Phys. 190 (1995) 345.
[40] L. Serrano-Andres, N. Forsberg, P.A. Malmqvist, J. Chem. Phys. 108 (1998) 7202.
[41] K. Takeshita, N. Shida, Chem. Phys. 210 (1996) 461.
[42] D. Xie, H. Guo, Chem. Phys. Lett. 307 (1999) 109.